DISPERSION ANALYSIS OF CROSS-DIPOLE DATA

Xiaojun Huang, Daniel R. Burns, and M. Nafi Toksöz

Earth Resources Laboratory
Department of Earth, Atmospheric, and Planetary Sciences
Massachusetts Institute of Technology
Cambridge, MA 02139

ABSTRACT

In this paper, we demonstrate that dispersion analysis of cross-dipole data has promising potential not only for differentiating stress-induced anisotropy from intrinsic anisotropy, but also for providing information on radial heterogeneity of formations. A dispersion analysis using improperly rotated data, however, exhibits spurious results because of the cross-contamination of the fast and slow flexural waves at different frequencies. When using Alford rotation, if the two orthogonal sources and/or receivers do not have matching signatures, the estimation of polarization directions of the split flexural waves will deviate from the actual directions, an important parameter that reflects vertical fracture orientation or regional stress direction. In addition, the two split flexural waves may not be separated completely. We present a new rotation scheme carried out in the frequency domain that takes into account signature mismatch of both the sources and the receivers. The new technique is applied to a set of four-component cross-dipole data from the Cymric Oil Field, and the estimated polarization direction of the fast flexural wave is compared with that from Alford rotation. The results show that the new rotation scheme yields the same trend as Alford rotation as a function of depth. However, at each depth, the results of these two methods can differ by as many as 50^o. Moreover, the length of the time window over which the new rotation method is applied has little effect on the crossover of dispersion curves, whereas Alford rotation is very sensitive to the time window length. Since the crossover of dispersion curves is an indicator of stress-induced anisotropy, the new rotation method offers advantages over standard Alford rotation.

INTRODUCTION

When borehole flexural waves travel through an azimuthally anisotropic formation, they are highly dispersive and split into two independently propagating wave types, usually referred to as fast and slow waves (Figures 1 and 2). Elastic anisotropy in rocks can be characterized as either intrinsic or stress-induced (Jaeger and Cook, 1977). Intrinsic anisotropy exists in the absence of external stresses. It can be caused by bedding, microstructure, or aligned fractures. Stress-induced anisotropy results from tectonic or overburden stress. A detailed investigation of aligned fractures is important in hydrocarbon production, and detailed knowledge of formation stresses would aid planning for stimulation treatments and predicting sand production and borehole stability. Thus, it is of great interest to separate stress-induced anisotropy from structural or intrinsic anisotropy of formations (Winkler *et al.*, 1998). A number of recent theoretical studies and laboratory experiments show that stress-induced anisotropy results in crossover of the dispersion curves of the two orthogonally polarized flexural waves, while intrinsic or structural anisotropy does not (Sinha *et al.*, 1994, 1996; Winkler *et al.*, 1994, 1998). Therefore, with broadband dipole data, the dispersion crossover can be used as an indicator of stress-induced anisotropy dominating over weak intrinsic or structural anisotropy (Winkler *et al.*, 1998). Nolte *et al.* (1997) developed a simple technique that provides an efficient scheme for estimating the dispersion curves of the fast and slow flexural waves from field data directly. Using this technique, we observe crossover of the fast and slow flexural waves from cross-dipole data from the Powder River Basin in Wyoming (Nolte *et al.*, 1997).

Cross-dipole logging usually does not provide pure fast and slow flexural waveforms directly; instead the two flexural waves are mixed in a complicated way in the data. Therefore, separating fast flexural waves from slow flexural waves is the first step in performing dispersive analysis. The most commonly used method is the rotation technique of Alford (1986), usually referred to as Alford rotation. This method rotates four-component data at a certain angle so as to align the orientations of the orthogonal sources/receivers with the polarization directions of fast and slow flexural waves. Zero cross-component energy suggests a perfect alignment in the sense that the pure fast and slow flexural waves are separated completely and the corresponding angle denotes the polarization of the flexural waves. Based on the assumption that source and receiver pairs are matched perfectly, this method works well in a variety of circumstances. However, it is usually the case that the signatures of the orthogonal source pairs are not matched, nor are the receiver responses (Hatchell and Cowles, 1992; Hatchell *et al.*, 1995). Using Alford rotation to analyze data from mismatched sources can lead to errors in the estimation of polarization azimuths and can give a mixture of fast and slow flexural waves on the diagonal components (Hatchell and Cowles, 1992). In this paper, we show that the mismatch of receiver response has the same effect. Besides Alford rotation, several other conventional rotation techniques, such as the linear transform technique (Li and Crampin, 1993), also neglect the effect of mismatched source signa-

tures and receiver responses. Hatchell and Cowles (1992) develop a technique that can handle mismatch of source signatures, but extra measurement is required from the field. We present a new rotation scheme carried out in the frequency domain that takes into account signature mismatch of both sources and receivers, while no extra measurements are needed. The new technique is applied to a set of four-component cross-dipole data from the Cymric Oil Field. The results show that the new rotation scheme yields the same trend as Alford rotation. However, at each depth, the estimation of fast flexural wave azimuth by the new rotation method differs from those of Alford rotation by up to 50^o. In addition, compared to Alford rotation (Nolte *et al.*, 1997), the length of the window over which the new rotation method is applied has little effect on the crossover of dispersion curves. Unfortunately, we are not able to do dispersive analysis using the data from the Cymric Oil Field because the data has too narrow a band to carry any meaningful dispersive information.

FLEXURAL DISPERSION AND FORMATION ANISOTROPY

In general, the dispersion of borehole flexural waves is caused by radial heterogeneity. Flexural waves are one type of borehole guided waves that are evanescent in the radial direction. With different wavelengths, flexural waves have different penetrating distances in the radial direction. Long wavelengths correspond to deeper penetration, thus deeper sampling to the formation. The phase velocity of the flexural wave is attributed to the velocity distribution of the region it samples. In general, at the high frequency limit, the wavelength is very short and has a very shallow penetration into the formation. Thus all the energy is confined within the borehole, and the phase velocity of the flexural wave has the velocity of the borehole fluid. At the low frequency limit, the flexural wave actually passes through the entire formation, and its phase velocity will be the effective formation shear velocity.

Typically, there are three sources of radial heterogeneity. The existence of the borehole itself, even in a homogeneous formation, often is the cause of flexural dispersion (Figure 3). As discussed above, in this case the phase velocity of the flexural wave will asymptotically be close to the fluid velocity at the high frequency limit and the formation shear velocity at the low frequency limit. The second cause of radial heterogeneity is radial heterogeneity of the formation (Figure 4). Again, at the high frequency limit the phase velocity of the flexural wave will be that of the borehole fluid velocity. However, as the frequency lowers, the flexural wave samples different regions of the formation and varies in frequency with the heterogeneity of the formation. Another cause of flexural dispersion is nonuniform stress distribution around the borehole, which is generally caused by tectonic stresses or an overburden. Figure 6 illustrates flexural dispersion due to uniaxial stress exerted on the borehole. In the absence of intrinsic anisotropy, the flexural wave has maximum velocity when its polarization is parallel to the direction of maximum compressive stress. It is interesting to note that that if a uniaxial compressive stress is applied in one direction, for instance at $\theta = 0^o$, compres-

sive stress concentration is present at $\theta = 90^o$ close to the borehole (Winkler *et al.*, 1998). Figure 6 shows the sum of principal stresses due to a unit uniaxial stress applied perpendicular to a borehole, along the $\theta = 0^o$ direction. The dotted curves in the region close to the borehole wall along $\theta = 0^o$ indicate tensile stresses, whereas the solid curves in the region perpendicular to the uniaxial stress direction denote large, compressive stresses. According to the dispersion analysis above, at low frequencies the fast flexural wave is polarized parallel to the far-field stress direction, while the slow flexural wave is polarized in the perpendicular direction. This is reversed at high frequencies, however, because the maximum compressive stress in the near-field is perpendicular to that of the far-field. This results in a crossover in the dispersion curves of these two flexural waves polarized orthogonally (Figure 5). This phenomenon is the consequence of the effect of stress concentration around the borehole. In the presence of intrinsic formation anisotropy, the principal direction will not change from far-field to near-field, thus no crossover will occur. With dispersion analysis and the crossover phenomenon, we are able to use the cross-dipole log to differentiate stress-induced anisotropy from intrinsic anisotropy.

A NEW ROTATION METHOD FOR MISMATCHED SOURCES AND RECEIVERS

In cross-dipole logging the fast and slow flexural waves are mixed in a complicated way in the data. Alford rotation works well when there is no mismatch of source signatures and receiver responses. It can separate the mixed flexural waves and find their polarization directions, which is an important parameter that indicates fracture orientation or stress direction. We define the four component data in a matrix form,

$$\underline{u}(t) = \begin{bmatrix} u_{xx}(t) & u_{yx}(t) \\ u_{xy}(t) & u_{yy}(t) \end{bmatrix} \tag{1}$$

and let θ be the angle between the direction of the fast flexural wave and the x-direction. Generally, Alford rotation takes the following form,

$$\underline{D} = \begin{bmatrix} \cos\theta & -\sin\theta \\ \sin\theta & \cos\theta \end{bmatrix} \underline{u}(t) \begin{bmatrix} \cos\theta & \sin\theta \\ -\sin\theta & \cos\theta \end{bmatrix}. \tag{2}$$

It takes θ as the fast flexural polarization direction when the energy of the cross-component vanishes, and it takes the two diagonal components as the two orthogonal flexural waveforms.

If there is a mismatch of source signatures and receiver responses, Alford rotation is no longer precise. The following rotation scheme is designed to eliminate the effects of a mismatch. Let $s_x(t)$ and $s_y(t)$ be source responses of the dipole oriented in the x-direction and y-direction, respectively. Let $g_f(t)$ and $g_s(t)$ be the dipole Green's function representing propagation from the source to the receiver location for fast and slow shear polarization directions. In other words, they are the Green's function that

contains dispersive properties of pure fast and slow flexural waves (Figure 7). For the x source, the components of the recorded wavefield can be written as a combination of the fast and slow flexural waves excited by the x source,

$$u_{xx}(t) = s_x(t) * g_f(t) * r_x(t)\cos^2\theta + s_x(t) * g_s(t) * r_x(t)\sin^2\theta \tag{3}$$

$$u_{yx}(t) = [-s_x(t) * g_f(t) * r_y(t) + s_x(t) * g_s(t) * r_y(t)]\sin\theta\cos\theta \tag{4}$$

where u_{ik} denotes the wavefield recorded on the i-component receiver for a source oriented in the k-direction; $r_x(t)$ and $r_y(t)$ denote the responses of the x-component and y-component receivers, respectively, and $*$ denotes convolution. Similarly, the wavefields for the y-source are,

$$u_{xy}(t) = [-s_y(t) * g_f(t) * r_x(t) + s_y(t) * g_s(t) * r_x(t)]\sin\theta\cos\theta \tag{5}$$

$$u_{yy} = s_y(t) * g_f(t) * r_y(t)\sin^2\theta + s_y(t) * g_s(t) * r_y(t)\cos^2\theta. \tag{6}$$

The purpose of all the rotation techniques is to determine the angle θ, and to recover pure fast and slow flexural waveforms, $g_f(t)$ and $g_s(t)$, respectively. The angle θ corresponds to shear polarization azimuth, an important measure that reflects vertical fracture orientation or regional stress direction.

We Fourier transform each of the four components and obtain

$$U_{xx}(\omega) = S_x(\omega)G_f(\omega)R_x(\omega)\cos^2\theta + S_x(\omega)G_s(\omega)R_x(\omega)\sin^2\theta \tag{7}$$

$$U_{yx}(\omega) = [-S_x(\omega)G_f(\omega)R_y(\omega) + S_x(\omega)G_s(\omega)R_y(\omega)]\sin\theta\cos\theta \tag{8}$$

$$U_{xy}(\omega) = [-S_y(\omega)G_f(\omega)R_x(\omega) + S_y(\omega)G_s(\omega)R_x(\omega)]\sin\theta\cos\theta \tag{9}$$

$$U_{yy}(\omega) = S_y(\omega)G_f(\omega)R_y(\omega)\sin^2\theta + S_y(\omega)G_s(\omega)R_y(\omega)\cos^2\theta. \tag{10}$$

We now combine these four components in a matrix $\underline{U}(\omega)$,

$$\underline{U}(\omega) = \begin{bmatrix} U_{xx}(\omega) & U_{yx}(\omega) \\ U_{xy}(\omega) & U_{yy}(\omega) \end{bmatrix} \tag{11}$$

then equations 7, 8, 9 and 10 may be written in matrix form,

$$\underline{U}(\omega) = \underline{R_{src}}(\omega,\theta)\underline{G}(\omega)\underline{R_{rec}}(\omega,\theta) \tag{12}$$

where

$$\underline{G}(\omega) = \begin{bmatrix} G_f(\omega) & 0 \\ 0 & G_s(\omega) \end{bmatrix} \tag{13}$$

and

$$\underline{R_{src}}(\omega,\theta) = \begin{bmatrix} S_x(\omega)\cos\theta & S_x(\omega)\sin\theta \\ -S_y(\omega)\sin\theta & S_y(\omega)\cos\theta \end{bmatrix} \tag{14}$$

$$\underline{R_{rec}}(\omega,\theta) = \begin{bmatrix} R_x(\omega)\cos\theta & -R_y(\omega)\sin\theta \\ R_x(\omega)\sin\theta & R_y(\omega)\cos\theta \end{bmatrix} \tag{15}$$

From equation 12, we obtain

$$\underline{G}(\omega) = \underline{R_{src}}^{-1}(\omega,\theta)\underline{U}(\omega)\underline{R_{rec}}^{-1}(\omega,\theta). \tag{16}$$

Equation 16 is the core of the new rotation method. It reveals that with mismatched source signatures and/or receiver responses, the rotation becomes nonorthogonal and varies from frequency to frequency even when the dipole sources and receivers and the fast and slow flexural waves are orthogonal. When and only when the cross-component energy of $\underline{G}(\omega)$ of equation 16 vanishes, we solve for the angle θ, and the two diagonal components of $\underline{G}(\omega)$ become pure fast and slow flexural waves, respectively.

As for Alford rotation, without considering the mismatch of source signatures and receiver responses, $S_x(\omega)$ is identical to $S_y(\omega)$ and $R_x(\omega)$ is identical to $R_y(\omega)$. If we denote $S(\omega)$ to be $S_x(\omega)$ or $S_y(\omega)$, and $R(\omega)$ to be $R_x(\omega)$ or $R_y(\omega)$, $\underline{R_{src}}(\omega,\theta)$ and $\underline{R_{rec}}(\omega,\theta)$ in equation 16 become,

$$\underline{R_{src}}(\omega,\theta) = S(\omega)\begin{bmatrix} \cos\theta & \sin\theta \\ -\sin\theta & \cos\theta \end{bmatrix} \tag{17}$$

$$\underline{R_{rec}}(\omega,\theta) = R(\omega)\begin{bmatrix} \cos\theta & -\sin\theta \\ \sin\theta & \cos\theta \end{bmatrix}. \tag{18}$$

Alford rotation rotates the four-component data orthogonally the same amount throughout the frequency band of the flexural waves. Alford rotation also takes the angle to be the shear azimuth when the cross-component energy of $\underline{G}(\omega)$ becomes zero. With any mismatch of source signatures and/or receiver responses, the angle obtained by Alford rotation will differ from the actual one, and the diagonal components of Alford rotation will not be pure fast and slow flexural waves, but rather a combination of them.

Without knowing the exact source signatures and receiver responses, the Green's functions of pure fast and slow flexural waves cannot be recovered exactly because they will be modified by one source signature and one receiver response. For convenience, equation 16 may be rewritten as

$$S_y(\omega)R_x(\omega)\begin{bmatrix} G_f(\omega) & \\ & G_s(\omega) \end{bmatrix} = \begin{bmatrix} \cos\theta/\alpha(\omega) & -\sin\theta \\ \sin\theta/\alpha(\omega) & \cos\theta \end{bmatrix}\underline{U}(\omega)\begin{bmatrix} \cos\theta & \sin\theta \\ -\sin\theta/\beta(\omega) & \cos\theta/\beta(\omega) \end{bmatrix} \tag{19}$$

where

$$\alpha(\omega) = \frac{S_x(\omega)}{S_y(\omega)} \tag{20}$$

denotes the ratio between the two orthogonal source signatures and

$$\beta(\omega) = \frac{R_y(\omega)}{R_x(\omega)} \tag{21}$$

denotes the ratio between the two orthogonal receiver responses. In an isotropic or VTI (transversely isotropic with vertical symmetry axis) formation, the two flexural waves will not split, which means $G_f(\omega) = G_s(\omega)$. Therefore, equations 7, 8, 9 and 10 will become

$$U_{xx}(\omega) = S_x(\omega)R_x(\omega) \tag{22}$$

$$U_{yx}(\omega) = 0 \tag{23}$$

$$U_{xy}(\omega) = 0 \tag{24}$$

$$U_{yy}(\omega) = S_y(\omega)R_y(\omega). \tag{25}$$

Intervals where both $u_{yx}(t)$ and $u_{xy}(t)$ vanish are the isotropic or VTI sections without flexural wave splitting. We may use $u_{xx}(t)$ and $u_{yy}(t)$ of the isotropic or VTI intervals to compute a parameter $\epsilon(\omega)$

$$\epsilon(\omega) = \frac{U_{xx}(\omega)}{U_{yy}(\omega)} = \frac{S_x(\omega)R_y(\omega)}{S_y(\omega)R_x(\omega)}. \tag{26}$$

Anisotropic intervals, where $u_{yx}(t)$ and $u_{xy}(t)$ are not zero, can be defined by another parameter, $\delta(\omega)$

$$\delta(\omega) = \frac{U_{yx}(\omega)}{U_{xy}(\omega)} = \frac{S_x(\omega)R_y(\omega)}{S_y(\omega)R_x(\omega)}. \tag{27}$$

$\epsilon(\omega)$ and $\delta(\omega)$ are parameters that describe tool properties, independent of formation type. Therefore, they remain constant throughout the logging. By further analysis, we obtain

$$\alpha(\omega) = \sqrt{\epsilon(\omega)\delta(\omega)} \tag{28}$$

$$\beta(\omega) = \sqrt{\delta(\omega)/\epsilon(\omega)} \tag{29}$$

which are used in the new rotation scheme in equation 19. Thus we determine θ and the fast and slow flexural waveforms.

APPLICATION TO FOUR-COMPONENT CROSS-DIPOLE DATA

We now apply our new rotation technique to estimate shear polarization azimuth from four-component cross-dipole data from the Cymric Oil Field. The data were acquired with a tool consisting of one pair of orthogonal dipole sources at the same depth point and an array of eight pairs of orthogonal dipole receivers with 0.5 foot spacing. The nearest receiver is 11 ft below the source. The data consists of 1024 samples for each receiver, and the sampling rate is $20\mu s$. Figure 8 shows a section of near-receiver waveforms in the cross-line direction. The pulse at 0.66 ms marks the start of the shot.

We use the short Fourier transform, a technique that is able to estimate the short-term, time-localized frequency content of a signal, to separate different modes contained in the recorded waveform. Figure 9 shows the spectrogram of the cross-line component nearest to the source at some depth. There are six peaks in the spectrum with central frequencies of 1 KHz, 2.5 KHz, 5 KHz, 14 KHz, 16 KHz and 20 KHz, and thus six modes are excited. The first arrival of the 1 KHz mode is around 7.2–0.66 ms, and the other five are around 2–0.66 ms. The source-receiver distance is 11 ft, therefore, the group velocity of the five modes is around 8209 ft/sec, which can be the compressional or tool modes, while the group velocity of the 1 KHz mode is around 1682 ft/sec, which we identify as the flexural mode. We apply a time window and a band-pass filter to the signal to separate the flexural mode. Thus we eliminate energy that comes earlier than 8 ms, is higher in frequency than 1.5 KHz and is lower in frequency than 0.5 KHz.

The interval shown in Figure 10, an isotropic section, is used to estimate $\epsilon(\omega)$. Anisotropic intervals are then used to estimate $\delta(\omega)$. With equations 28 and 29, $\alpha(\omega)$ and $\beta(\omega)$ can be estimated. $\alpha(\omega) = S_x(\omega)/S_y(\omega)$, which represents the ratio of the two orthogonal sources, is the average of all the intervals and receivers, and $\beta(\omega) = R_y(\omega)/R_x(\omega)$, representing the ratio of the two orthogonal receivers, is the average of all the intervals. By averaging through intervals, the effect of formation heterogeneity on $\alpha(\omega)$ and $\beta(\omega)$ are removed. For perfectly matched source pairs and receiver pairs, $\alpha(\omega)$ and $\beta(\omega)$ should be united at all frequencies. Therefore, there should be a single point in the plots of the real and imaginary part of $\alpha(\omega)$ and $\beta(\omega)$. In fact, $\alpha(\omega)$ and $\beta(\omega)$ from our data are quite scattered, as shown in Figures 11 and 12. This scattering implies that the signatures of the two orthogonal sources and the responses of the two orthogonal receivers are mismatched differently at different frequencies. Points that are far from the dense part of the plots in Figures 11 and figure 12, are probably due to some measurement error or formation heterogeneity between the receivers. When considering their contribution to cross-component energy, we assign smaller weighting factors to the frequencies of these points than those of dense points. Thus we have a more robust inversion. We use the following objective function to estimate polarization of flexural waves,

$$f(\omega,\theta) = \sum_{all\,frequencies} \left[D_{12}^2(\omega,\theta) + D_{21}^2(\omega,\theta)\right] \lambda(\omega) \tag{30}$$

where $\lambda(\omega)$ is the weighting factor.

Figures 13 and 14 show a section of fast shear azimuth from both Alford rotation and the new scheme. At some intervals, Alford rotation fails to determine the fast shear azimuth but instead finds the slow shear azimuth, which is 90^o different. If we ignore this effect, fast shear azimuth from both methods have the same trend; however, at each depth, the two results may differ by up to 50^o. The energy ratio $E_{cross}/E_{diagonal}$ is less than 20% for Alford rotation, and less than 5% for the new rotation method.

EFFECTS OF ROTATION ON DISPERSION ANALYSIS

The crossover phenomenon in dispersion curves can be used as an indicator of stress-induced anisotropy only when it is assured that the two dispersion curves represent the two flexural waves polarized in the principal directions. If the rotation process fails to estimate the polarization direction of the two principal flexural waves accurately, the two principal flexural waves cannot be separated completely. Nolte *et al.* (1997) noticed that Alford rotation depends strongly only the length of the time window over which it is applied. Figure 15 shows four-component cross-dipole data recorded by the receiver pair closest to the source pair and the Alford rotation results with respect to different time window lengths (10, 20, 30, 40 and 50 samples). The corresponding estimates of the fast flexural wave polarization direction using Alford rotation, 45^o, 40^o, 35^o, 75^o and 20^o, respectively, vary with the time window length. As Nolte *et al.* (1997) discuss, due to flexural wave dispersion, lower frequencies are associated with higher velocities, and thus arrive earlier in the data, while higher frequencies arrive later. Time windowing, therefore, cuts out some of the high frequency content of the flexural waves, and thus some of the near field information. Figure 6 shows that the closer the stress contour is to the borehole, the the smaller it is. When time windows with different lengths are applied, the sensitivity of the data to the principal polarization directions varies, and thus the estimation results vary. For the purpose of dispersion analysis, we suggest that the rotation be carried out in the frequency domain because no time windowing is involved in the frequency domain. If there are zeros in the spectrum, a small constant number may be added to the spectrum to ensure numerical stability, and that is known as pre-whitening in seismic data processing (Yilmaz, 1997).

Because Alford rotation does not take into account the fact that mismatched source and receiver signatures affect the data as a function of frequency, it may not yield accurate estimates of principal polarization directions. Accordingly, Alford rotation may not separate the two principal flexural waves completely, and there may be spurious crossover in dispersion curves. Figure 16 shows dispersion analysis results for a single depth of four-component data. Using Alford rotation, we rotate the data by 20^o, 35^o, 40^o, 45^o, and 75^o, respectively. Dispersion behavior, especially the crossover phenomenon, varies considerably with respect to different rotation angles. Therefore, rotation is a crucial step in applying the crossover phenomenon to differentiate stress-induced anisotropy from intrinsic anisotropy.

CONCLUSIONS

Dispersion analysis of cross-dipole data provides a potential method not only for differentiating stress-induced anisotropy from intrinsic anisotropy, but also provides information on the radial heterogeneity of formations. A robust rotation scheme is a crucial step in such an analysis. Standard Alford rotation cannot incorporate any mismatch of source signatures and receiver responses. In addition, time windowing the signal in

Alford rotation can degrade accuracy. As a result, spurious crossover may occur in dispersion curves. In this paper, we present a new rotation technique that takes into account mismatched source signatures and receiver responses, which can be estimated from the data. In addition, since it is a frequency domain method, time windowing, which gives rise to some complications in Alford rotation, is no longer an issue.

ACKNOWLEDGMENTS

Many thanks go to Dr. Gopa S. De of Chevron Petroleum Technology Co. for many helpful discussions.

This work was supported by the Borehole Acoustics and Logging/Reservoir Delineation Consortia at the Massachusetts Institute of Technology.

REFERENCES

Alford, R.M., 1986, Shear data in the presence of azimuthal anisotropy, *56th Ann. Internat. Mtg., Soc. Explor. Geophys., Expanded Abstracts*, 476–479.

Hatchell, P.J. and Cowles, C.S., 1992, Flexural borehole modes and the measurement of azimuthal anisotropy, *62nd Ann. Internat. Mtg., Soc. Explor. Geophys., Expanded Abstracts*, 201–204.

Hatchell, P.J., De, G.S., Winterstein, D.F., and DeMartini, D.C., 1995, Quantitative comparison between a dipole log and VSP in anisotropic rocks from the Cymric Oil Field, California, *65th Ann. Int. Mtg., Soc. Eplor. Geophys., Expanded Abstracts*, 13–16.

Jaeger, J.C. and Cook, N.G.W., 1977, *Fundamentals of Rock Mechanics,* Halsted Press.

Li, X.Y. and Crampin, S., 1993, Linear-transform techniques for processing shear-wave anisotropy in four-component seismic data, *Geophysics, 59*, 176–191.

Nolte, B., Rao, R., and Huang, X., 1997, Dispersion analysis of split flexural waves, *Borehole Acoustics and Logging/Reservoir Delineation Consortia Annual Report,* MIT, 12-1–12-26.

Sinha, B.K. and Kostek, S., 1996, Stress-induced anisotropy in borehole flexural waves, *Geophysics, 61*, 1899–1907.

Sinha, B.K., Plona, T.J., Winkler, K.W., and D'Angleo, R.M., 1995, Stress-induced dipole anisotropy in a dry Berea sandstone, *65th Ann. Int. Mtg. Soc. Expl. Geophys., Expanded Abstracts*, 22–25.

Winkler, K.W., Sinha, B.K., and Plona, T.J., 1998, Effects of borehole stress concentrations on dipole anisotropy measurements, *Geophysics, 63*, 11–17.

Winkler, K.W., Plona, T., Hsu, C.-J., Sinha, B. K., and Kostek, S., 1994, Effects of borehole stress concentrations on dipole anisotropy measurements, *64th Ann. Int. Mtg. Soc. Expl. Geophys., Expanded Abstracts*, 1136–1138.

Yilmaz, O., 1997, *Seismic Data Processing,* Society of Exploration Geophysics.

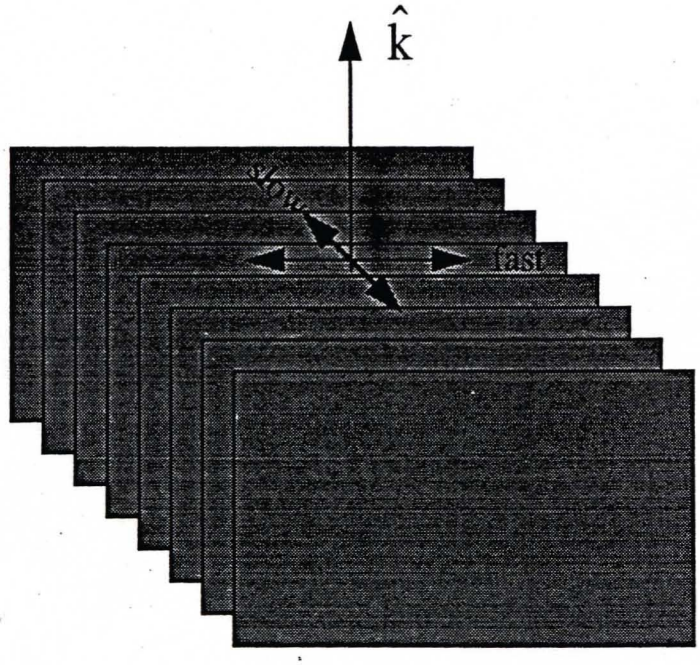

Figure 1: Aligned vertical fractures, known as VTI medium. 'Fast' and 'slow' denote the polarization directions of fast and slow shear waves, respectively.

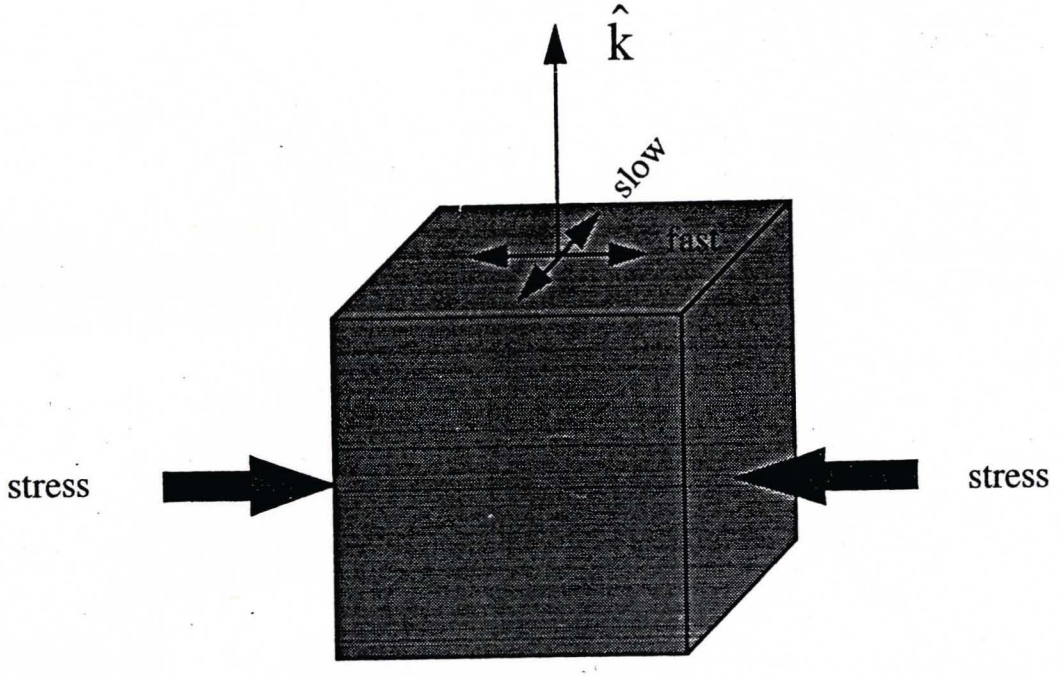

Figure 2: Homogeneous elastic formation under uniaxial stress also exhibits azimuthal anisotropy. 'Fast' and 'slow' denote the polarization directions of fast and slow shear waves, respectively.

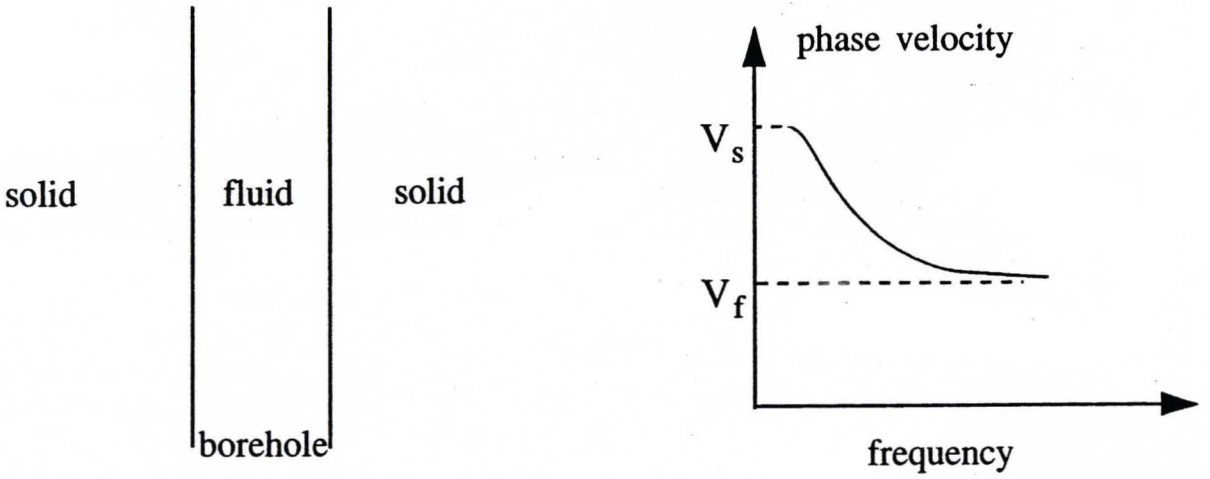

Figure 3: Existence of the borehole itself causes dispersion of all guided waves.

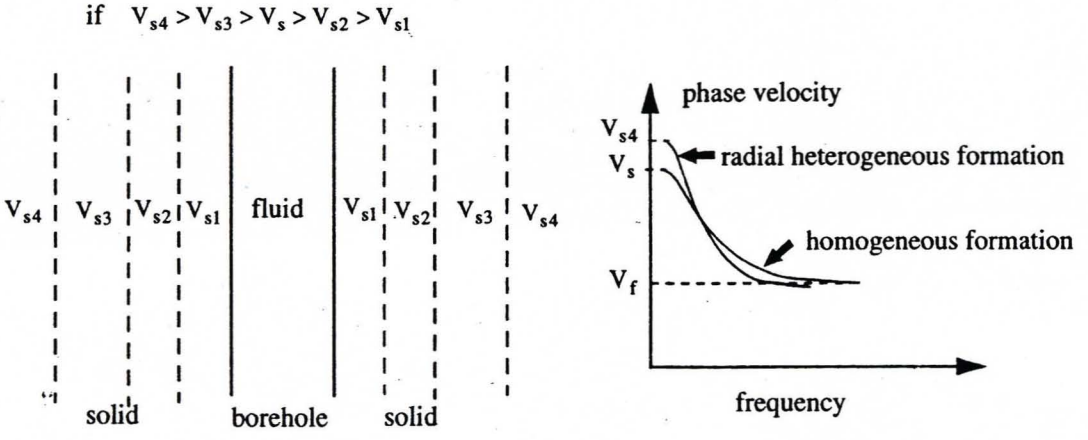

Figure 4: Radial heterogeneity of the formation causes dispersion of guided waves.

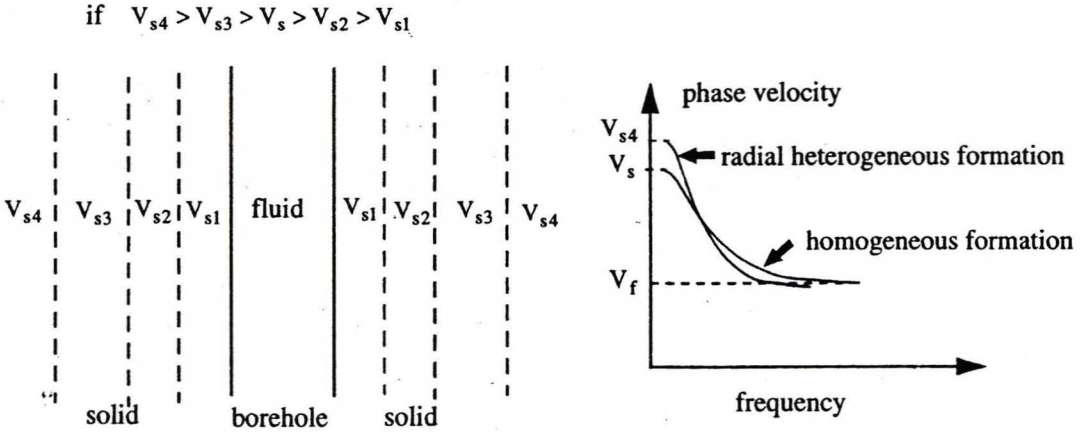

Figure 4: Radial heterogeneity of the formation causes dispersion of guided waves.

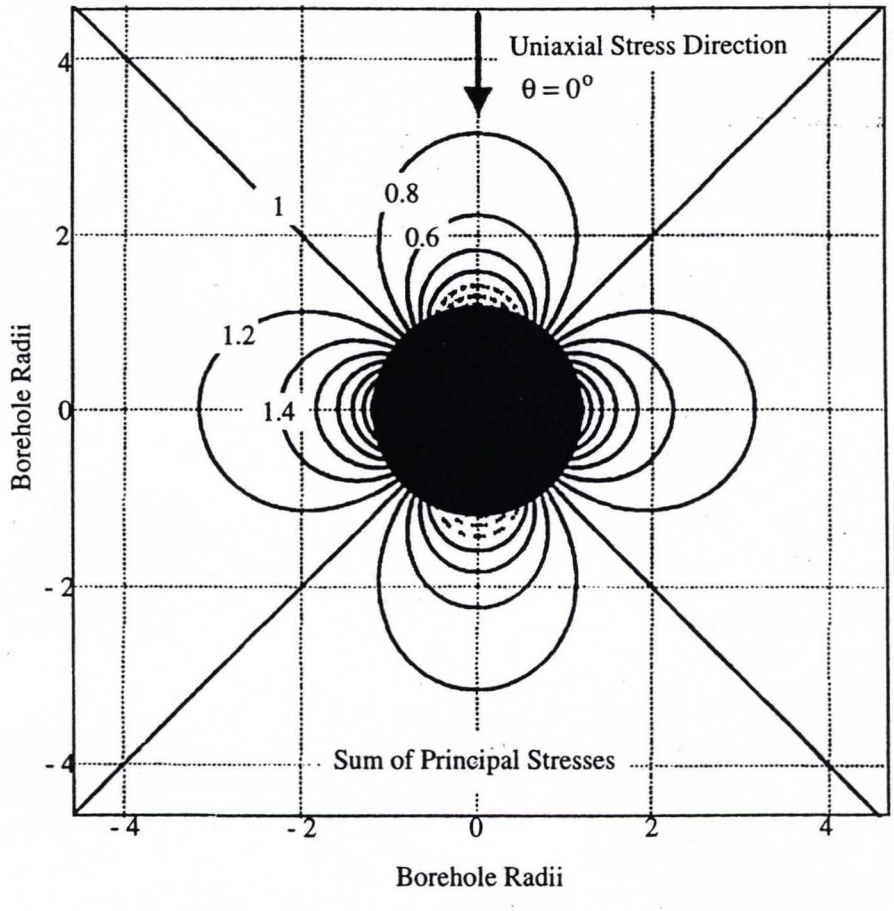

Figure 6: Contour map of the sum of principal stresses induced by a unit uniaxial stress applied along the $\theta = 0^o$ direction. Compressive stress concentrations develop at $\pm 90^o$ to the applied stress. Tensile stress concentrations (dashed contours) develop near the borehole at 0^o and 180^o.

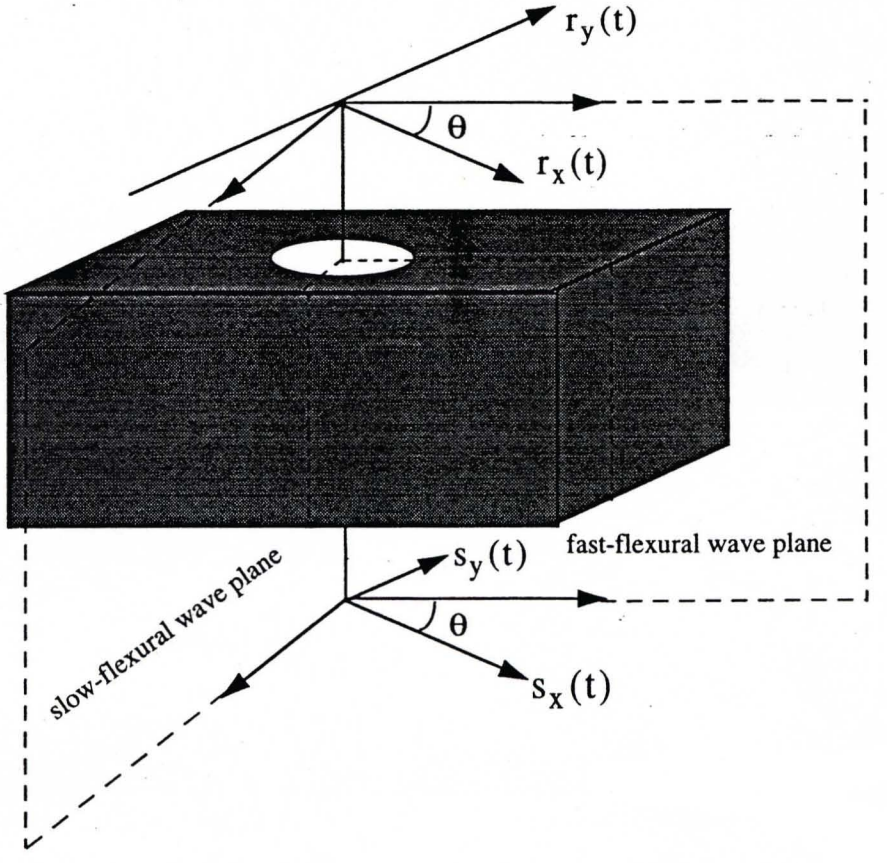

Figure 7: Flexural wave splitting in cross-dipole logging. θ is the angle between the direction of the fast flexural wave and the x-direction. $s_x(t)$ and $s_y(t)$ are source responses and $r_x(t)$ and $r_y(t)$ are receiver responses of the dipole oriented in the x-direction and y-direction, respectively.

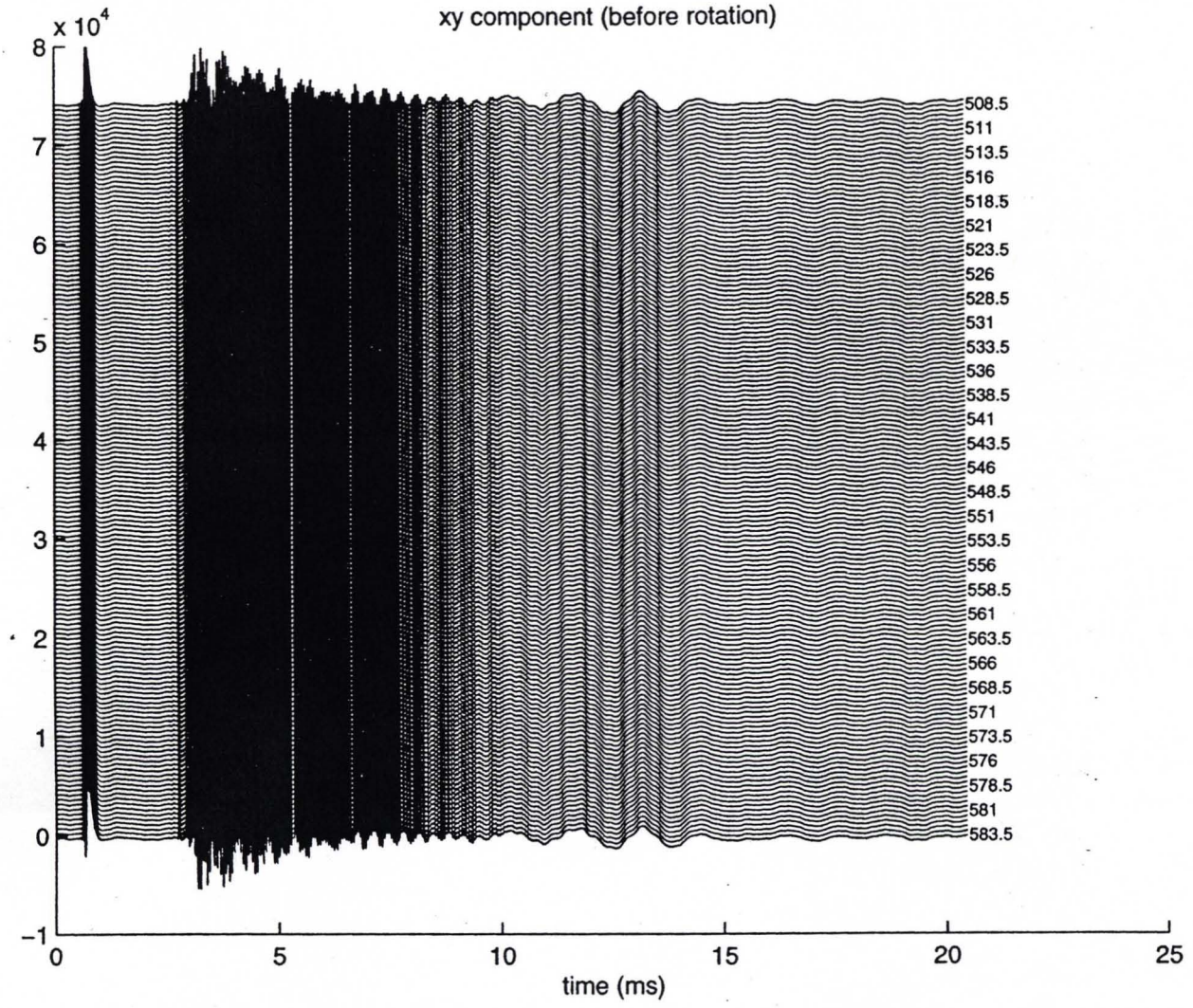

Figure 8: A section of a cross-line measurement of cross-dipole waveforms from the Cymric Oil Field, recorded by the receiver that is closest to the source.

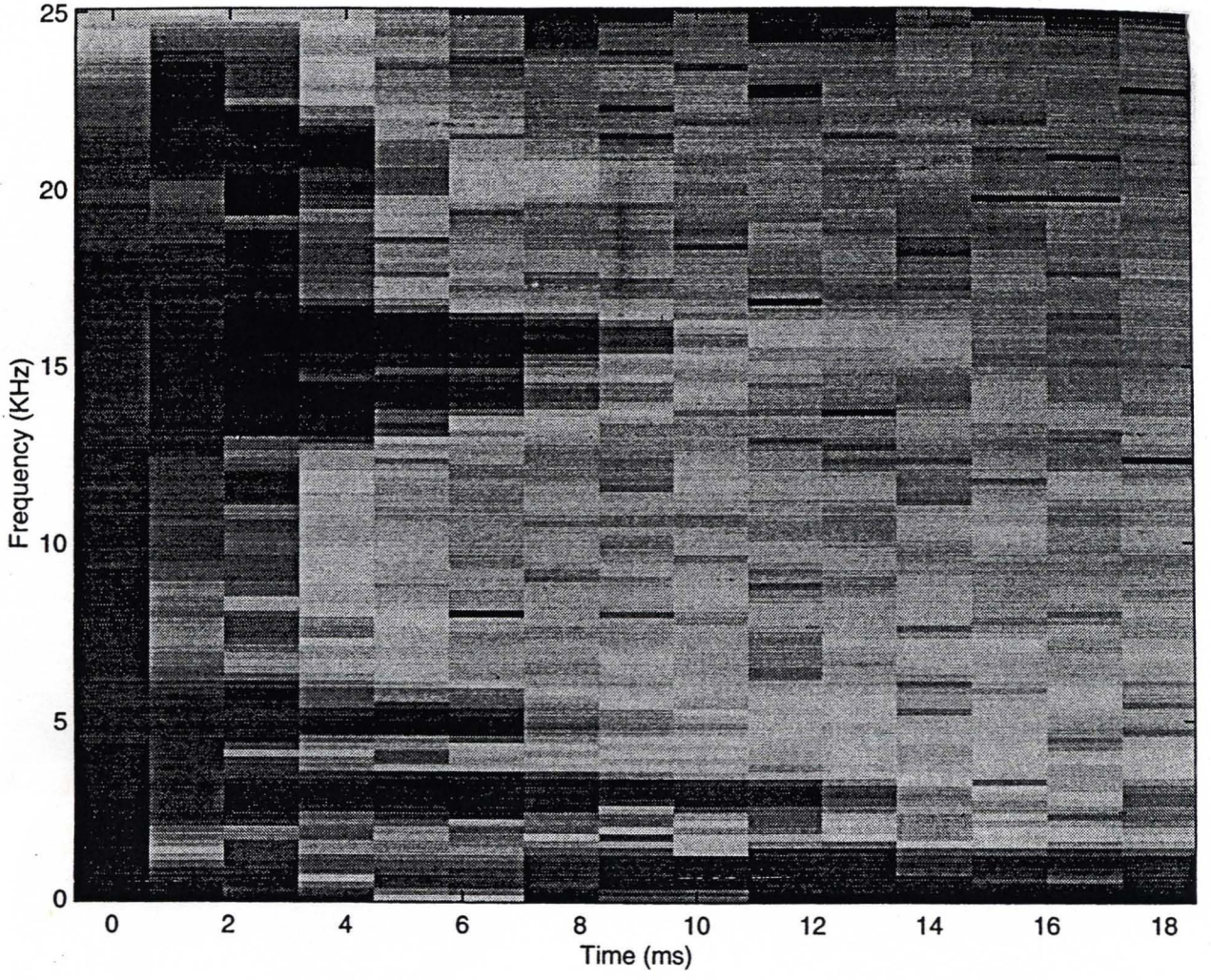

Figure 9: Spectrogram of one cross-line component at some depth. FFT points: 256, time window length 128, overlap points: 64.

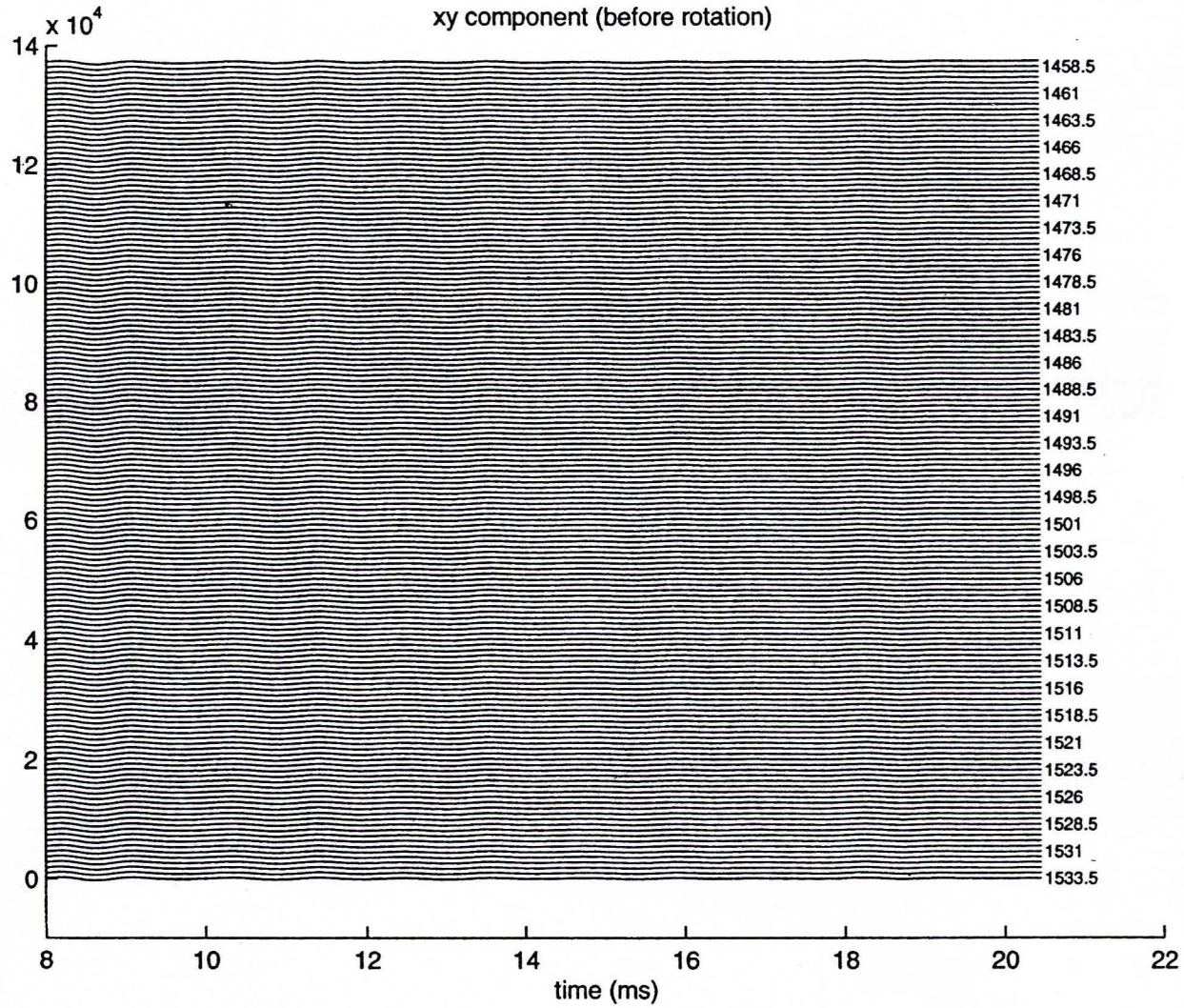

Figure 10: Isotropic section used for the estimation of $\epsilon(\omega)$.

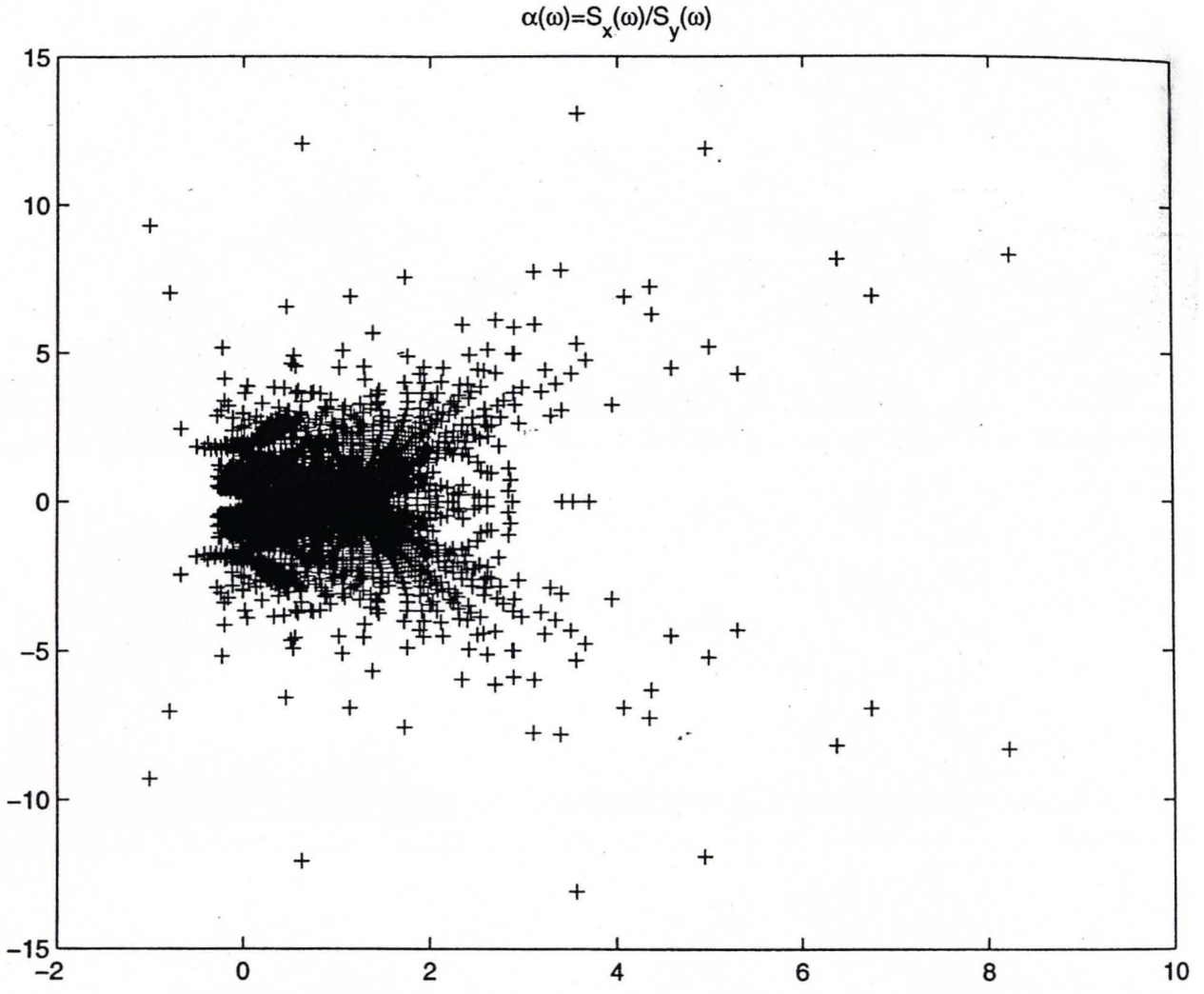

Figure 11: Estimation of $\alpha(\omega) = S_x(\omega)/S_y(\omega)$. The horizontal axis is the real part of α and the vertical axis denotes the imaginary part of α. Each point in the figure corresponds to a frequency.

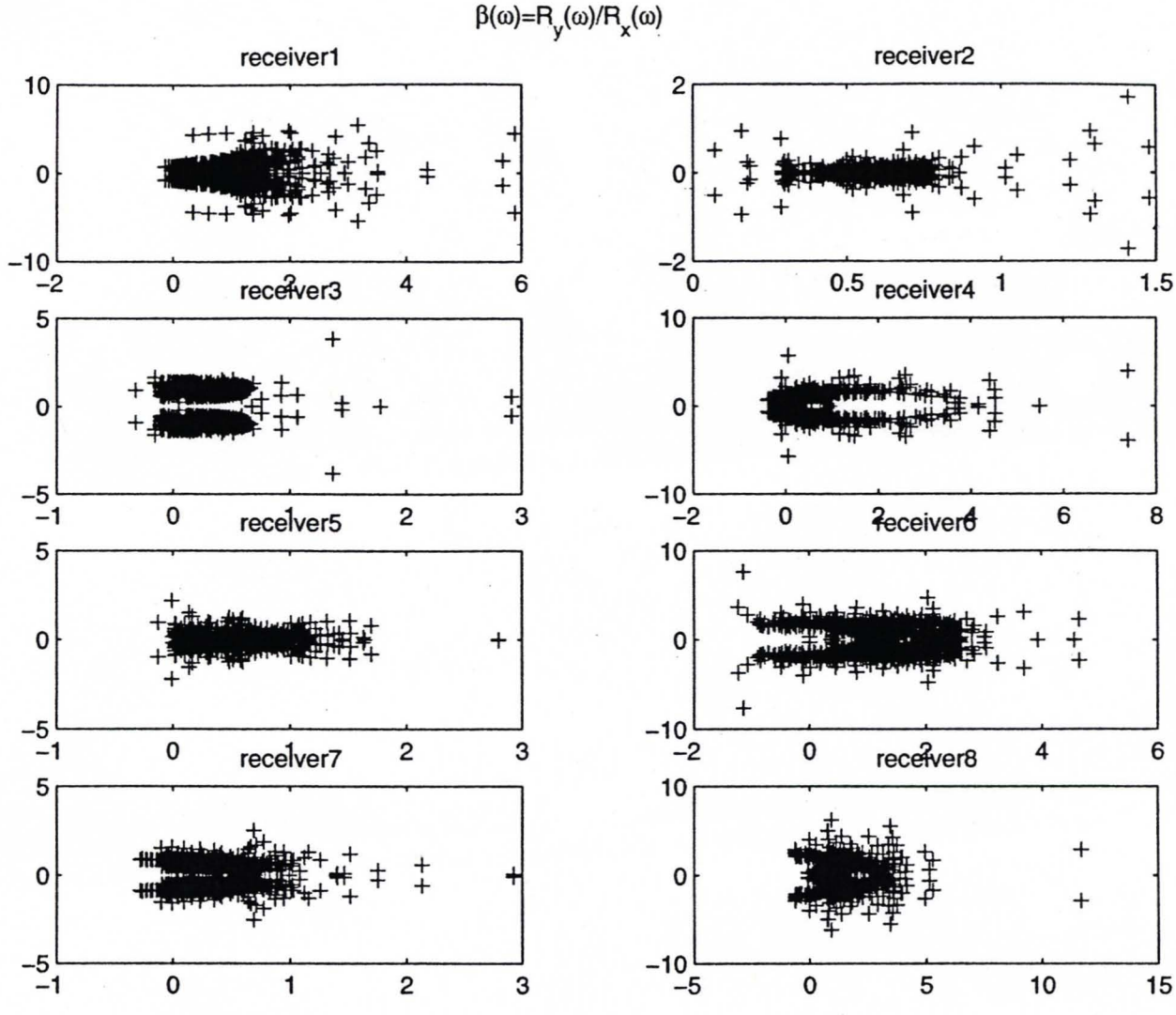

Figure 12: Estimation of $\beta(\omega) = R_x(\omega)/R_y(\omega)$. The x axis denotes the real part of $R_x(\omega)/R_y(\omega)$, while the y axis represents the imaginary part of $R_x(\omega)/R_y(\omega)$. Each point in the figures corresponds to a frequency.

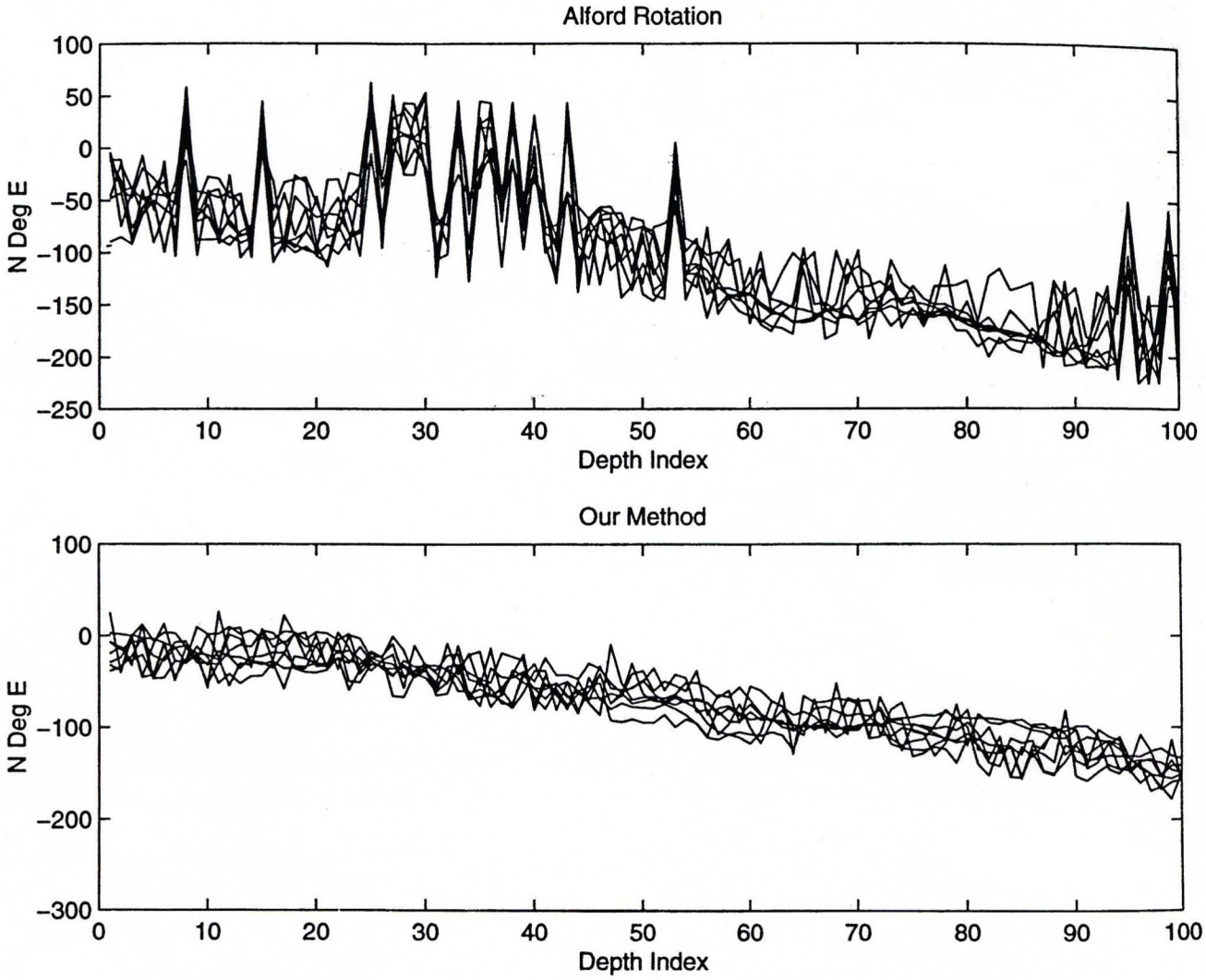

Figure 13: The azimuth of one principal direction estimated by Alford rotation and the new scheme.

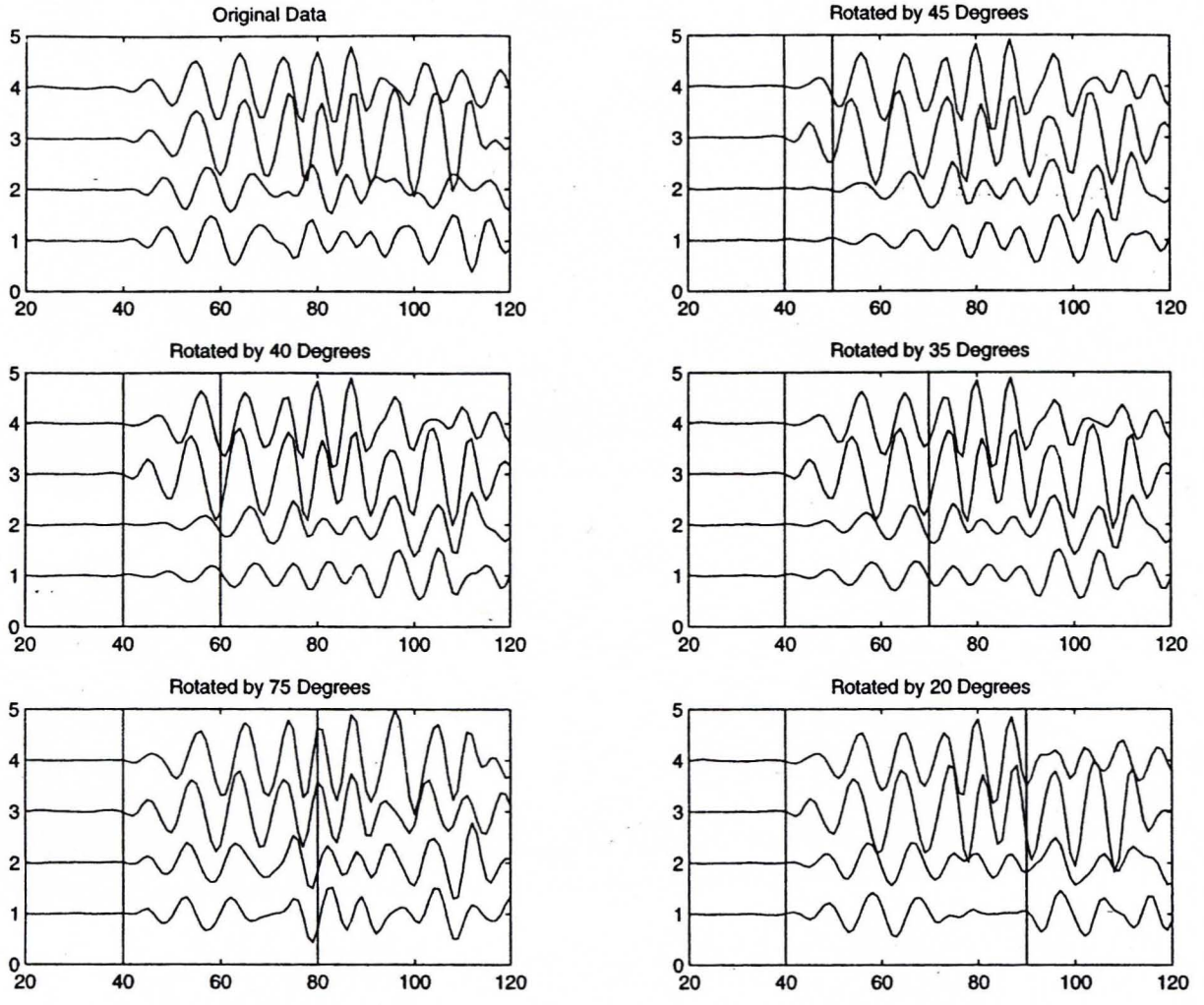

Figure 14: The average azimuth of one principal direction estimated by Alford rotation and the new scheme.

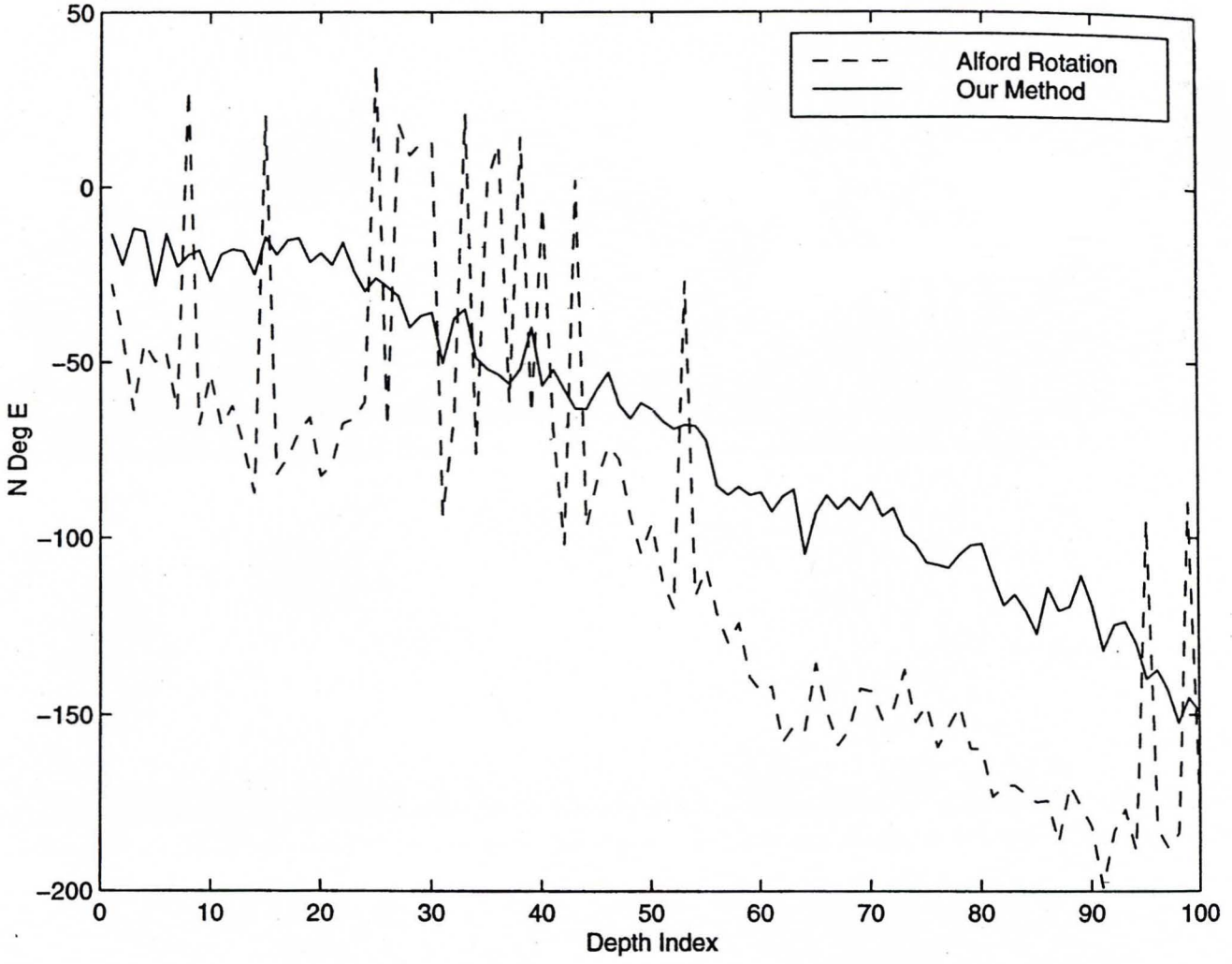

Figure 15: Four-component cross-dipole data recorded by the receiver pair closest tot he source pair and its Alford rotation results with respect to different time window lengths (10, 20, 30, 40, and 50 samples). The corresponding estimates of the fast flexural wave polarization direction using Alford rotation are 45^o, 40^o, 35^o, 75^o, and 20^o, respectively. The time window is indicated by vertical lines in each plot.

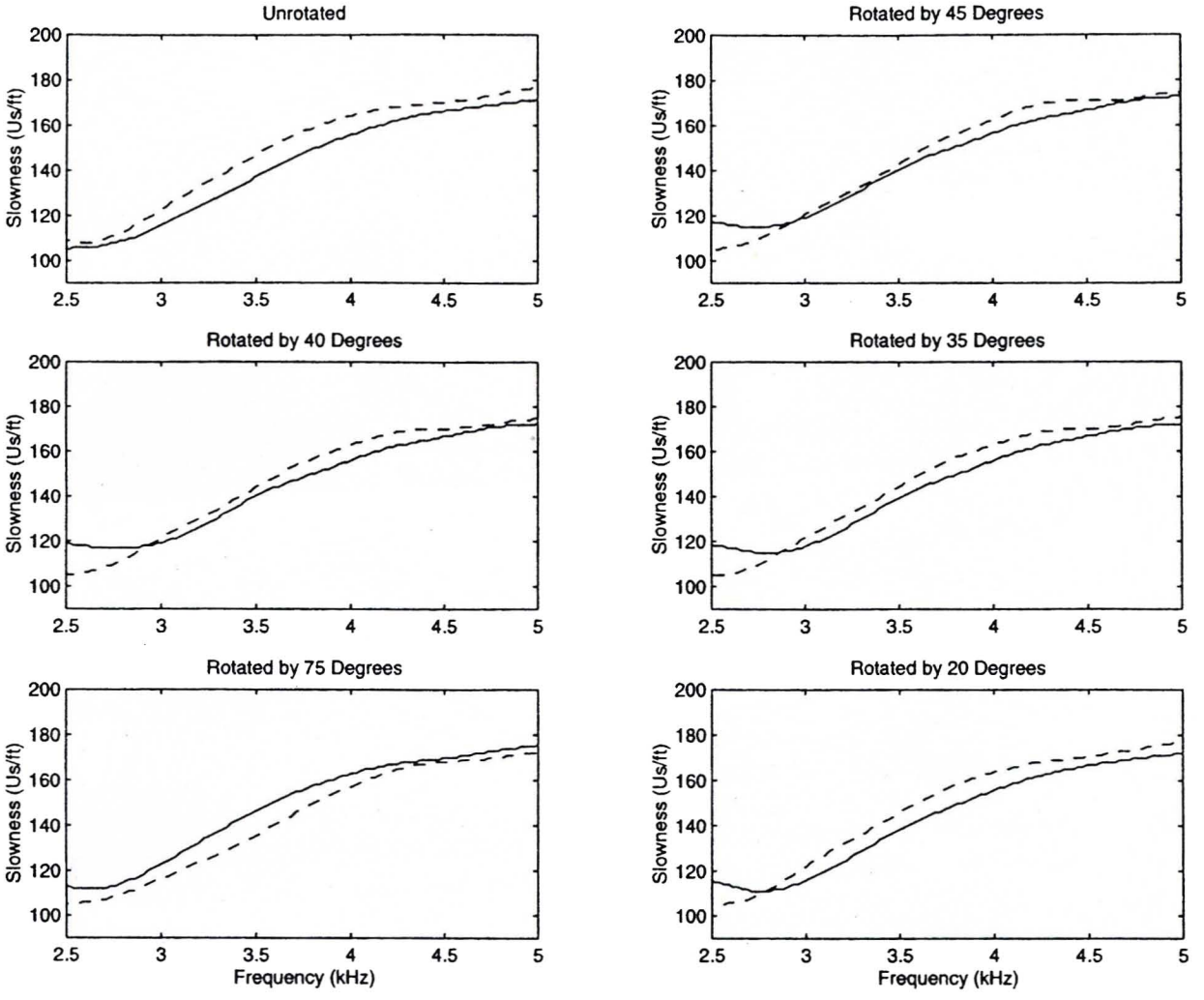

Figure 16: Dispersion curves of the two flexural waves measured on the diagonal components of the unrotated data and of the data rotated to the angles of 20^o, 35^o, 40^o, 45^o, and 75^o.